Theoretical study of the dissociative recombination of HeH^+

Hidekazu Takagi*
Center for Natural Science, Kitasato University, 1-15-1 Kitasato, Sagamihara, Kanagawa, 228-8550 Japan
(Received 26 February 2003; revised manuscript received 19 April 2004; published 26 August 2004)

The dissociative recombination (DR) of HeH^+ is studied using the multichannel quantum defect theory (MQDT) of molecules. The MQDT is extended to include the dissociative Rydberg states. The idea of a "closed dissociative channel" is introduced for a precise description. The calculated DR cross section sensitively depends upon rotational motion, which enhances the DR at a collision energy lower than 0.2 eV. Calculations in the present study reproduced the DR rate coefficient measured by two facilities of storage rings (CRYRING and TARN II). A great change of the adiabatic quantum defect with internuclear distance induced a large DR cross section in the noncrossing system. This mechanism is an alternative to the electronic resonance of the crossing existing system.

DOI: 10.1103/PhysRevA.70.022709 PACS number(s): 34.80.Lx

I. INTRODUCTION

Dissociative recombination (DR) consists of two successive stages. First, an excited molecule is formed by recombination of an incident electron, and it is then subsequently stabilized by dissociation. The most probable molecular excited state is a two-electron or multiple-electron excited resonance state [1]. The potential curve crossing between the ion and resonance states enhances the electron recombination because of the strong interaction between different electronic configurations. This also stabilizes the resonance state due to quick dissociation. Thus, potential curve crossing is a factor that can yield a large DR cross section. However, such a curve crossing is absent in the DR of HeH^+ at the energies of a thermal electron [2]. The dissociative states of HeH^+ are Rydberg states, in which electronic configurations are single-electron excited states, the same as the initial state. Since the Rydberg states are orthogonal to the initial state under the fixed nuclei approximation, a nonadiabatic interaction (NAI) must drive the DR. As the NAI did not seem to be as strong as the electronic configuration interaction, the low-energy DR cross section of HeH^+ had been supposed to be small compared with the DR to which the potential curve crossing contributes.

Nevertheless, the large cross section has been revealed by both experimental [3] and theoretical [4–6] studies. One experiment was conducted using the beam storage ring, called the CRYRING. Several theoretical studies were based on the *R*-matrix method [6] or the multichannel quantum defect theory (MQDT) [4,5]. Although these theoretical calculations successfully reproduced the order of a DR cross section, the consistency with the experiment was not satisfactory. For example, it seems difficult to explain well the difference between the $^3HeH^+$ and $^4HeH^+$ by these theoretical studies.

Another theoretical study adopting the MQDT has succeeded in reproducing the energy dependence of the experimental cross section for four isotopes $^3HeH^+$, $^4HeH^+$, $^3HeD^+$, and $^4HeD^+$ [7]. The experiment was conducted using the storage ring called TARN II. In the present study, we will provide more details of a previous paper's theoretical study [7].

The present approach is based on the MQDT, which was used in Guberman's studies [4,5]. Guberman classified the electronic states of neutral molecules into two groups. One consists of the three lowest states *X*, *A*, and *C*, which are regarded as the dissociative states. The other group consists of the higher Rydberg and ionizing states, which are supposed to be molecular bonding states. He took into account the NAI between those two groups. Using the "two-step method" by Giusti [8], he first made the eigenstates diagonalize the NAI and then estimated the other NAI between the Rydberg and ionizing states using the MQDT. In the present study, we recognize all states to be Rydberg states. We shall uniformly represent the vibrational and dissociative states of the Rydberg states. The present study includes the rotational motion, which is neglected in some previous studies. This means that we take into account the dynamical mixing of angular momentum in the electronic and nuclear motions. As the *X* state is not a Rydberg state, the coupling with the *X* state should be coped with another method, as Guberman proposed. We here neglect the contribution of the *X* state to the DR for simplicity because the measured kinetic energy of DR fragment atoms indicates that the contribution of the *X* state is small [3,9,10].

In the present study, we shall also answer an important question: why the DR cross section is large even when the potential curve crossing is absent. The MQDT with rotational and vibrational motion has been well established [11–13]. We here utilize the method proposed in the previous study by Takagi [13], which is referred to as I hereafter.

II. MQDT WITH A DISSOCIATIVE CHANNEL

We here consider an extension of the MQDT to include the dissociative states of the Rydberg manifolds, of which the

*Electronic address: takagi@kitasato-u.ac.jp

nuclear kinetic energy is higher than the vibrational states. In order to treat the dissociative state as a vibrational state, the continuum nuclear states $\chi^{\mathsf{E}}_{\varepsilon}(R)$ are discretized:

$$\chi^{\mathsf{S}}_{j}(R) = \frac{1}{\sqrt{\Delta}}\int_{\varepsilon_j-\Delta/2}^{\varepsilon_j+\Delta/2} \chi^{\mathsf{E}}_{\varepsilon}(R)d\varepsilon \tag{1}$$

$$\simeq \sqrt{\Delta}\chi^{\mathsf{E}}_{\varepsilon_j}(R), \tag{2}$$

where R is the internuclear distance, ε is the kinetic energy of nuclear relative motion, and ε_j with integer j denotes the jth discretized energy of which the interval is Δ. The value of Δ is small enough to regard $\chi^{\mathsf{E}}_{\varepsilon}(R)$ as independent of ε in that interval. The superscripts S and E on the wave functions, respectively, denote the normalization with "state" and "energy." Using Eq. (1) and the definition of normalization by energy,

$$\int \chi^{\mathsf{E}}_{\varepsilon_j}(R)\chi^{\mathsf{E}}_{\varepsilon_{j'}}(R)dR = \delta_D(\varepsilon_j - \varepsilon_{j'}), \tag{3}$$

we can confirm the normalization as

$$\int \chi^{\mathsf{S}}_{j}(R)\chi^{\mathsf{S}}_{j'}(R)dR = \delta_{jj'}, \tag{4}$$

where δ_D is Dirac's delta function and $\delta_{jj'}$ is Kronecker's delta. The inner region of the MQDT is represented using basis functions of the discretized dissociative functions besides the usual vibrational functions. We hereafter use the symbol j for unifying the discretized dissociative state and vibrational state. Using the basis functions, we trace the MQDT for the DR according to I.

As the first step, we consider the electron scattering by a molecular ion. We impose the boundary conditions for electrons according to the MQDT. We use the following symbols for the angular momentum and its azimuthal component: N^+, M^+ for the rotation of the molecular ion, ℓ^+, m^+ for the slow electron, and J, M for the total system.

We also use $\mu(R)$ to represent the adiabatic quantum defect (AQD), $M(R)$ to represent the mixing matrix between partial waves of incident electrons, and $\tilde{\ell}$ to denote the eigenchannel diagonalizing this mixing. The electronic angular momentum around the molecular axis is denoted by Λ for a neutral molecule and Λ^+ for an ion molecule. The suffix $+$ is given for the quantum numbers of the ion molecule. The Jost function representing the half collision from the inner region to the outer region is expressed in the following form from Eq. (A.1) of I:

$$(\mathcal{J}_{\pm})^{JM}_{j^+N^+M^+\ell^+m^+,\Lambda} = \sqrt{\frac{2N^+ + 1}{2J+1}}C(\ell^+N^+J;m^+M^+M)C(\ell^+N^+J;\Lambda-\Lambda^+,\Lambda) \times\sum_{j\tilde{\ell}} \langle \chi^{\mathsf{S}N^+\Lambda^+}_{j^+}|e^{\mp i\pi\mu_{\tilde{\ell}\Lambda}(R)}M_{\ell^+\tilde{\ell}}(R)|\chi^{\mathsf{S}J\Lambda}_{j}\rangle. \tag{5}$$

In the above equation, we adopted the notation given by Rose [14] for the Clebsh-Gordan coefficient C. We can find the inverse matrix of the above function as follows:

$$(\mathcal{J}^{-1}_{\pm})^{JM}_{\Lambda,j^+N^+M^+\ell^+m^+} = \sqrt{\frac{2N^+ + 1}{2J+1}}C(\ell^+N^+J;m^+M^+M)C(\ell^+N^+J;\Lambda-\Lambda^+,\Lambda) \times\sum_{j\tilde{\ell}} \langle \chi^{\mathsf{S}J\Lambda}_{j}|M_{\ell^+\tilde{\ell}}(R) * e^{\pm i\pi\mu_{\tilde{\ell}\Lambda}(R)}|\chi^{\mathsf{S}N^+\Lambda^+}_{j^+}\rangle. \tag{6}$$

According to Seaton [15], an S matrix is given by

$$\mathbf{S} = \mathcal{X}_{oo} - \mathcal{X}_{oc}[\mathcal{X}_{cc} - e^{-2\pi i\nu_c}]^{-1}\mathcal{X}_{co}, \tag{7}$$

with

$$\mathcal{X} = \mathcal{J}_{-}\mathcal{J}_{+}^{-1}, \tag{8}$$

where the subscript o (c) indicates open (closed) channels, and ν is the effective principal quantum number. If we do not identify the final rotational states, the cross section is given by

$$\sigma_{j^{+\prime},j^+N^+} = \frac{\pi}{k^2}\rho\sum_{JM}\sum_{N^{+\prime}}\sum_{\ell^{+\prime}m^{+\prime}}\frac{1}{2N^+ + 1}\left|\sum_{\ell^+}\sqrt{2\ell^+ + 1}i^{\ell^+} \times S^{JM}_{j^{+\prime}N^{+\prime}M^{+\prime}\ell^{+\prime}m^{+\prime},j^+N^+M^+\ell^+}(m^+ = 0)\right|^2. \tag{9}$$

Here, $k = \sqrt{2\epsilon}$ is the wave number of the incident electron and ρ is the ratio of the multiplicity of the final state to that of the initial state. $\rho = 1$ for the DR of HeH^+. In Eq. (9), the summation on M^+ and $M^{+\prime}$ must not be taken because of the restriction $M = m^{+\prime} + M^{+\prime} = M^+$.

As in I, we represent the cross section using the reduced S matrix $\tilde{\mathbf{S}}$, which is given by Eqs. (7) and (8) replacing the Jost function $\mathcal{J}$ with the reduced Jost function $\tilde{\mathcal{J}}$. The $\tilde{\mathcal{J}}$ is defined by extracting the azimuthal factor from $\mathcal{J}$ as follows:

$$(\mathcal{J}_{\pm})^{JM}_{j^+N^+M^+\ell^+m^+,\Lambda} = C(\ell^+N^+J;m^+M^+M)(\tilde{\mathcal{J}}_{\pm})^{J}_{j^+N^+\ell^+,\Lambda}. \tag{10}$$

The S matrix given by Eq. (7) then becomes

$$\mathbf{S}^{JM}_{j^{+\prime}N^{+\prime}M^{+\prime}\ell^{+\prime}m^{+\prime},j^+N^+M^+\ell^+(m^+=0)} = C(\ell^{+\prime}N^{+\prime}J;m^{+\prime}M^{+\prime}M)\tilde{\mathbf{S}}^{J}_{j^{+\prime}N^{+\prime}\ell^{+\prime},j^+N^+\ell^+} \times C(\ell^+N^+J;m^+M^+M), \tag{11}$$

as proved in the Appendix of I. Putting the above equation into Eq. (9), we can obtain a formula of the cross section after elementary calculations:

$$\sigma_{j^{+\prime},j^+N^+} = \frac{\pi}{k^2}\rho\sum_{J}\sum_{N^{+\prime}}\sum_{\ell^{+\prime}\ell^+}\frac{2J+1}{2N^+ + 1}\left|\tilde{\mathbf{S}}^{J}_{j^{+\prime}N^{+\prime}\ell^{+\prime},j^+N^+\ell^+}\right|^2. \tag{12}$$

For numerical calculations, using the reactance matrix **R** is more convenient than the *S* matrix because **R** is real. The reduced *S* matrix can be related to the reduced reactance matrix $\tilde{\mathbf{R}}$ in the same way as **S** to **R**. Furthermore, $\tilde{\mathbf{R}}$ is expressed in terms of its smoothed matrix $\tilde{\mathcal{R}}$, according to the MQDT by Seaton [15]. That is,

$$\tilde{\mathbf{R}} = \tilde{\mathcal{R}}_{oo} - \tilde{\mathcal{R}}_{oc}(\tilde{\mathcal{R}}_{cc} + \tan \pi\nu)^{-1}\tilde{\mathcal{R}}_{co}. \tag{13}$$

The matrix $\tilde{\mathcal{R}}$ is written in the following form using the reduced Jost function $\tilde{\mathcal{J}}_{\pm}$ defined in Eqs. (10) and (5):

$$\begin{aligned}\tilde{\mathcal{R}}^{J}_{j^{+\prime}N^{+\prime}\ell^{+\prime},j^{+}N^{+}\ell^{+}} &= -i\{(\tilde{\mathcal{J}}_{-} - \tilde{\mathcal{J}}_{+})(\tilde{\mathcal{J}}_{-} + \tilde{\mathcal{J}}_{+})^{-1}\}^{J}_{j^{+\prime}N^{+\prime}\ell^{+\prime},j^{+}N^{+}\ell^{+}} \\ &= \sum_{\Lambda} \langle N^{+\prime}|\Lambda\rangle^{J\ell^{+\prime}\Lambda^{+}} \sum_{\tilde{\ell}} \langle \chi^{SN^{+\prime}\Lambda^{+}}_{j^{+\prime}} | M_{\ell^{+\prime}\tilde{\ell}}(R) \tan \pi\mu_{\tilde{\ell}\Lambda}(R) M_{\tilde{\ell}\ell^{+}}(R) | \chi^{SN^{+}\Lambda^{+}}_{j^{+}} \rangle \langle \Lambda|N^{+}\rangle^{J\ell^{+}\Lambda^{+}}. \end{aligned} \tag{14}$$

The factor $\langle \Lambda | N^{+} \rangle$ introduced by Jungen and Atabek [11] is represented by

$$\langle \Lambda | N^{+} \rangle^{J\ell^{+}\Lambda^{+}} = \sqrt{\frac{2N^{+}+1}{2J+1}} C(\ell^{+}N^{+}J; \Lambda - \Lambda^{+}, \Lambda^{+}). \tag{15}$$

After calculating $\tilde{\mathbf{R}}$, we shall have the cross section of Eq. (12) through the matrix $\tilde{\mathbf{S}}$ from the well-known relation $\tilde{\mathbf{S}} = (\mathbf{1} - \tilde{\mathbf{R}})^{-1}(\mathbf{1} + \tilde{\mathbf{R}})$.

The above formulation is originally valid for bounded nuclear motion. In order to extend it to include the dissociative processes, it is necessary to impose a continuum boundary condition for nuclear motion.

The MQDT analytically imposes the boundary condition to the electronic wave function, and we shall impose the condition to the total system consisting of electrons and nuclei according to the physical situation.

The discretized dissociative Rydberg states are identified by (ε_j, ν), where ν is the effective quantum number of the Rydberg state. When the ε_j satisfies the energy conservation law, the state (ε_j, ν) becomes a real dissociative channel—i.e., an open channel. The energy conservation law is represented in atomic units by

$$\varepsilon_j - \frac{1}{2\nu^2} = E_{v^{+}N^{+}} + \epsilon, \tag{16}$$

where $E_{v^{+}N^{+}}$ is the initial rotational-vibrational energy, and ϵ is the collision energy, which is regarded equivalent to the energy of the incident electron. In the present case, this law is satisfied if ν equals the principal quantum number n of the dissociated hydrogen atoms. On the other hand, unless $\nu = n$, it becomes a closed channel because there are no channels satisfying energy conservation. We call those dissociative channels "closed dissociative channels" (CDC's) [16]. Closed channels other than CDC's are formed by the Rydberg state associated with the vibrational state (v^{+}, ν).

The normalization of a real dissociative Rydberg state $(\nu = n)$ must be changed. The function $\chi^{S}_{j}(R)$ in Eq. (14) changes to $\chi^{E}_{\varepsilon_j}(R)$, where $\chi^{E}_{\varepsilon_j}(R) = \Delta^{-1/2}\chi^{S}_{j}(R)$ with $\varepsilon_j = E_v + \epsilon + \frac{1}{2}n^{-1/2}$. At the same time, the normalization of the electronic state must be changed to the state normalization because this channel is electronically closed. The electronic basis functions adopted in the MQDT are basically the Coulomb wave functions normalized by energy. Since the state density for the Rydberg state (ν) is ν^3, the relation between the electronic wave functions normalized by state $\phi^{S}(r)$ and by energy $\phi^{E}(r)$ becomes $\phi^{S}(r) = \nu^{-3/2}\phi^{E}(r)$. The normalization factor adds up to $\Delta^{-1/2}\nu^{-3/2}$ for the real dissociative Rydberg channel. For the CDC's, this factor is 1 (unity) since the boundary condition is automatically imposed by the MQDT.

In a double continuum state like dissociative excitation (DE), there is arbitrariness in the choice of the observing flux. If we observe the fragment atoms and do not see the free electrons, an atomic flux must be chosen. In this case, the energy normalization must be adopted to the nuclear motion, which gives the normalization factor $\Delta^{-1/2}$. The associated electronic state must be normalized by the state in order to avoid the double-continuum problem. The normalization factor of an electronic state is $\Delta^{1/2}$. This normalization is equivalent to the electronic states that are averaged over the energy interval Δ. The total normalization factor is 1. When we observe the electrons in the DE, that factor is also 1.

As the result of imposing the boundary condition on the total system, the smoothed reactance matrix elements $\tilde{R}^{J}_{j^{+\prime}N^{+\prime}\ell^{+\prime},j^{+}N^{+}\ell^{+}}$ of Eq. (14) become the ones multiplied by the factor $\Delta^{-1/2}\nu^{-3/2}$ at each time the initial or final state is the real dissociative Rydberg state. Using this modified matrix $\tilde{\mathcal{R}}$ instead of Eq. (14), we can obtain the DR cross section

$$\sigma^{DR}_{\varepsilon,v^{+}N^{+}} = \frac{\pi}{k^2}\rho \sum_{J} \sum_{N^{+\prime}} \sum_{\ell^{+\prime}\ell^{+}} \frac{2J+1}{2N^{+}+1} |\tilde{\mathbf{S}}^{J}_{\varepsilon N^{+\prime}\ell^{+\prime},v^{+}N^{+}\ell^{+}}|^2, \tag{17}$$

where v^{+} denotes the initial vibrational state.

III. DETAILS OF THE CALCULATIONS

A. Asymptotic behavior of the quantum defect

In general, the AQD value does not become zero (+ integer) at the large internuclear distance *R*. Thus the integrant

of R in Eq. (14) does not always become zero even at a large R. In the present study, we consider the function $F(R)$ whose value becomes a nonzero constant F_o at $R \geqslant R_o$. The integration of Eq. (14) can be written as:

$$\begin{aligned}\tilde{\mathcal{R}}^{J}_{j^+{}'N^+{}'\ell^+{}',j^+N^+\ell^+} &\equiv \int_0^\infty \chi^{\mathrm{S}}_{j^+{}'} F(R) \chi^{\mathrm{S}}_{j^+} dR \\ &= \int_0^{R_o} \chi^{\mathrm{S}}_{j^+{}'} [F(R) - F_o] \chi^{\mathrm{S}}_{j^+} dR + F_o \delta_{j^+{}'j^+} \\ &= \Delta \int_0^{R_o} \chi^{\mathrm{E}}_{\varepsilon_{j^+{}'}} [F(R) - F_o] \chi^{\mathrm{E}}_{\varepsilon_{j^+}} dR + F_o \delta_{j^+{}'j^+}.\end{aligned} \tag{18}$$

The magnitude per unit energy of the diagonal matrix elements can be written as

$$\frac{\tilde{\mathcal{R}}_{j^+N^+{}'\ell^+{}',j^+N^+\ell^+}}{\Delta} = \int_0^{R_o} \chi^{\mathrm{E}}_{\varepsilon_{j^+}} [F(R) - F_o] \chi^{\mathrm{E}}_{\varepsilon_{j^+}} dR + \frac{F_o}{\Delta}, \tag{19}$$

which diverges with $1/\Delta$ when $\Delta \to 0$. This divergence is brought by the continuum-continuum interaction at a large R. This divergent part physically represents elastic electron scattering by the dissociating ion. Thus, this divergence is rooted in the double-continuum problem. The only and easiest way to avoid the divergence is to cut the interaction beyond a certain large internuclear distance. Especially, in the inner region of the MQDT, the values of a quantum defect at a large R are meaningless. Therefore, we cut off the adiabatic quantum defect at a large R by a manner of not affecting the final result in the question. Two examples of such cutting are shown in the $p\sigma$ quantum defect of Fig. 1. We shall see that the DR cross section is not sensitive to these two cutting manners.

B. Jump of the quantum defect

Figure 1 displays the AQD of s, $p\sigma$, and $p\pi$ Rydberg states, of which the lowest states are, respectively, called the A, C, and B states. The marks in the figure indicate the AQD deduced from the phase shift calculated by Sarpal [18] using the R-matrix method. That is, the AQD is equal to (phase shift at zero collision energy)/π. The lines in Fig. 1 show the interpolation and extrapolation of those AQD's, which are employed in the present calculation. We adopted the fourth-order Lagrangian interpolation and the Padè [2, 2] approximation for the extrapolation. Since the values at a large R should be zero (+ integer), as discussed in Sec. III A, there remains considerable arbitrariness, especially on the extrapolation, in the $p\sigma$ state. Two typical examples of the extrapolation are given in Fig. 1 by solid and dashed curves, which were generated by adding different artificial values at a large R. The AQD of $p\sigma$ drastically changes when crossing the value of 0.5, where the principal quantum number changes one unit. The principal quantum number of the C state changes from 2 to 3 with R decreasing. This AQD feature can be confirmed by the bound-state calculation of the C state [17].

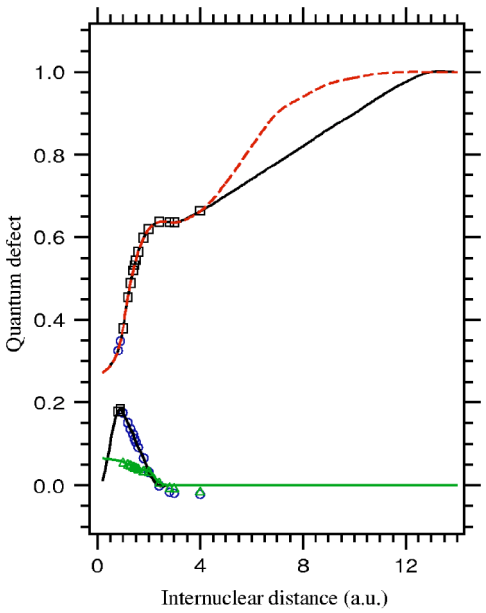

FIG. 1. Adiabatic quantum defect. The marks the calculation by Sarpal [18] for the s (○), $p\sigma$ (□), and $p\pi$ (△) states. The curves indicate those values employed in the present calculation.

Since the integrand of Eq. (14) diverges at $\mu(R) = \pm 0.5$, no numerical integration method can work unless this singularity is removed. The right-hand side of Eq. (14), denoted here by I, is regarded as an integration on R. We can clarify the singularity of I by letting $x = \cos \pi\mu(R)$:

$$\begin{aligned}I &\equiv \int_0^\infty G(R) \tan \pi\mu(R) dR \\ &= -\int_{\cos \pi\mu(0)}^{\cos \pi\mu(\infty)} G(R) \left(\pi \frac{d\mu(R)}{dR} \right)^{-1} \frac{1}{x} dx,\end{aligned} \tag{20}$$

where $G(R)$ is the part of I other than $\tan \pi\mu(R)$. Since the above equation contains a first-order singularity at $x = 0$, we can remove this singularity by the usual numerical integration method. Putting

$$g(x) = -G(R) \left(\pi \frac{d\mu(R)}{dR} \right)^{-1}, \tag{21}$$

we can rewrite the integration as

$$I = \int_{\cos \pi\mu(0)}^{\cos \pi\mu(\infty)} dx \left(\frac{g(x) - g(0)}{x} \right) dx - g(0) \int_{\cos \pi\mu(0)}^{\cos \pi\mu(\infty)} \frac{1}{x} dx \tag{22}$$

$$= I_0 - g(0) \log \left| \frac{\cos \pi\mu(0)}{\cos \pi\mu(\infty)} \right|, \tag{23}$$

where the integrand in I_0 has no singularity. By returning it to the original variable, we obtain a representation for I_0 as

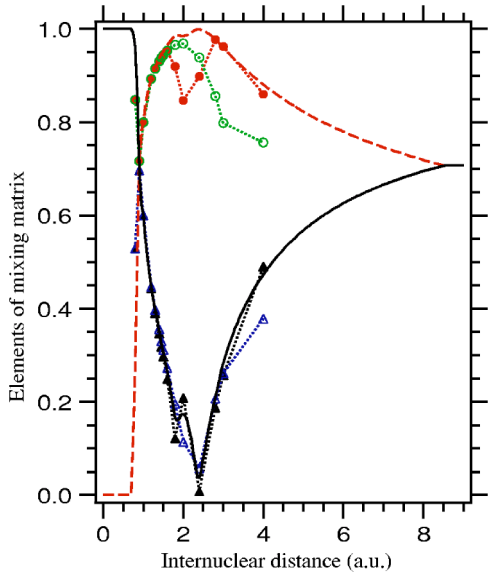

FIG. 2. The diagonal (triangle) and off-diagonal (circle) elements of mixing matrix **M**, which were calculated by Sarpal [18]. The black marks indicate the eigenstates of the *s* character, and the open marks represent the $p\sigma$ one. The solid and dashed curves, respectively, indicate the diagonal and off-diagonal matrix elements deduced by Eqs. (26) and (25) as mentioned in the text.

$$I_0 = \int_0^\infty \tan \pi\mu(R) \times \left\{ G(R) - G(R_0) \left(\frac{d\mu(R)}{dR} \right)_{R_0}^{-1} \frac{d\mu(R)}{dR} \right\} dR, \quad (24)$$

where R_0 is defined by $\cos \pi\mu(R_0)=0$. Using Eqs. (23) and (24), we can obtain an accurate integral value, although numerical differentiation of AQD's on R is required.

C. Mixing matrix

The ADQ behavior illustrated in Fig. 1 indicates a strong interaction between the *s* and $p\sigma$ states near $R=0.9$ a.u. The avoided crossing is seen between the AQD curves, where the characters of angular momentum are interchanged with each other at the crossing point. In the present study, we only consider the coupling between the *s* and $p\sigma$ partial waves. Since the mixing matrix is unitary, it is identified by a single parameter called the mixing parameter χ [19]:

$$\mathbf{M} = \frac{1}{\sqrt{1+\chi^2}} \begin{pmatrix} 1 & \chi \\ -\chi & 1 \end{pmatrix}. \quad (25)$$

In general, the matrix element $M_{i,j}$ represents the fraction of the partial wave i in the eigenstate j. We now make the *s* and $p\sigma$ waves to be $i=1$ and 2, respectively. The matrix elements deduced from Sarpal's result is not fully symmetric, as shown in Fig. 2, since partial waves more than two are employed in his calculation. Especially at a large R more than 2.0 a.u., the contribution of the $d\sigma$ wave to the $p\sigma$ eigenstate becomes significant. However, we neglected the $d\sigma$ wave because its AQD is far smaller than the $p\sigma$'s AQD at every R. Thus, we adopted the mean value of Sarpal's result by setting the mixing parameter as

$$\chi = \frac{M_{12} - M_{21}}{M_{11} + M_{22}}, \quad (26)$$

where all $M_{i,j}$, $i,j=1,2$, are given by Sarpal. The adopted mixing matrix in the present calculation is deduced by Eq. (25), putting in the value obtained by Eq. (26). These matrix elements are also shown in Fig. 2.

TABLE I. The atomic mass values adopted in the present calculation. The values are presented as the ratio of nuclei to the electron mass.

	$^1H^+$	$^2H^+$	$^3He^{2+}$	$^4He^{2+}$
m_{nucl}/m_e	1836.15	3670.48	5495.88	7294.30

D. Condition of the calculation

We adopted the ground-state potential energy curve of HeH^+ calculated by Kołos and Peek [20]. The error of this potential energy curve is no more than 0.6 meV, according to the comparison with another calculation [21].

In the present calculation, we took account of the rotational states $N^+ \leqslant 10$ and all of the existing vibrational states. We also considered the *s*, $p\sigma$, and $p\pi$ partial waves of the incident electron. In this condition, a change of the rotational state is limited to $|N^{+\prime} - N^+| \leqslant 2$ in our MQDT model.

The mass ratios of nuclei to electrons, m_{nucl}/m_e, are listed in Table I, which are obtained from the fundamental physical constants [23]. The calculated vibrational energy levels of isotopes agree with the latest experiment [22] within 0.1 meV for the rotational and vibrational (v) transitions of $v=0 \rightarrow 1$. This difference amount is made by adding only the mass of one electron to the reduced mass of two nuclei. This means that the adopted potential has almost the same accuracy as the limit of the Borm-Oppenheimer approximation. In other words, the energetic error of the present calculation is larger than 0.1 meV.

The interval of discretized energy, Δ, and the energy region covered by those adopted discretized functions are given in Table II for each isotope. Those intervals are smaller than the smallest level spacing of the vibrational states. The values of the covered region determine the maximum dissociation energies. They fully cover the dissociative channel of $He(1s^2)+H(n=2)$ and higher-*n* channels at a collision energy lower than 1.0 eV when the target ion is in the vibrational ground state.

TABLE II. Energy interval of the discretized dissociative states and their covering energy region.

	$^3HeH^+$	$^4HeH^+$	$^3HeD^+$	$^4HeD^+$
Interval (a.u.)	0.0007	0.0007	0.001	0.0014
Covered region (a.u.)	0.112	0.112	0.160	0.1764

E. Convolution

The DR cross section has a fine resonance structure, which often disturbs recognizing the cross-section magnitude. In the following section, we shall discuss the mechanism of the nonadiabatic DR processes and investigate them in comparison to the experimental result. For this purpose, we show the relationship between the true cross section and the observed one in the storage ring experiment. The derivation of this relationship and details of its characteristics will be published elsewhere. Here, we only show the result related to the present study.

The observed rate coefficient is represented by the convolution of the true cross section $\sigma(E)$ as the following:

$$Y^{obs}(E_o) = \sqrt{\frac{2}{\pi m}}\frac{1}{kT_\perp}\sqrt{\frac{1}{kT_\parallel}}\int_0^\infty dE E\sigma(E)I(E,E_o), \tag{27}$$

where E is the collision energy, E_o is the collision energy set in the experiment, T denotes the temperature of electron fluctuations for longitudinal (indicated by $\parallel$) and transverse ($\perp$) directions to the beam axis of the storage ring, m is the reduced mass of the collision system, and k is the Boltzmann constant. Using the error function

$$\mathrm{erf}(x) = \frac{2}{\sqrt{\pi}}\int_0^x \exp(-s^2)ds, \tag{28}$$

the weight function of convolution is represented as

$$I(E,E_o) = \frac{1}{2}\sqrt{\frac{\pi k T_\perp T_\parallel}{E(T_\perp - T_\parallel)}}\exp\left\{\frac{E_o}{k(T_\perp - T_\parallel)} - \frac{E}{kT_\perp}\right\} \times\{\mathrm{erf}(\beta) - \mathrm{erf}(\alpha)\}, \tag{29}$$

where

$$\begin{pmatrix}\alpha\\ \beta\end{pmatrix} = \mp\sqrt{\frac{E}{k}\left(\frac{1}{T_\parallel} - \frac{1}{T_\perp}\right)} - \sqrt{\frac{E_o}{kT_\parallel}}\sqrt{\frac{T_\perp}{T_\perp - T_\parallel}}. \tag{30}$$

The observed cross section $\sigma^{obs}(E_o)$ is given by

$$\sigma^{obs}(E_o) = \sqrt{\frac{1}{\pi}}\frac{1}{kT_\perp}\sqrt{\frac{1}{kT_\parallel}}\frac{1}{\sqrt{E_o}}\int_0^\infty dE\, E\sigma(E)I(E,E_o). \tag{31}$$

If the cross section is sharply distributed at the energy $E = E_r$—that is, if $\sigma(E) = \sigma(E_r)\delta_D(E - E_r)$—the above equation becomes Eq. (7) in the paper of Danared [24]. Equation (31) is the convolution formula using Danared's equation as the impulse response function.

IV. RESULT AND DISCUSSION

A. DR cross section of $^4HeH^+$

Figure 3 illustrates the calculated DR cross section of $^4HeH^+$ ($v^+ = 0, N^+ = 0$). In order to depend on the interval of discretized energy, Δ, the calculation with a twice interval ($\Delta = 0.0014$ a.u. $= 38$ meV) is also shown in the figure. Even the large interval calculation is almost convergent.

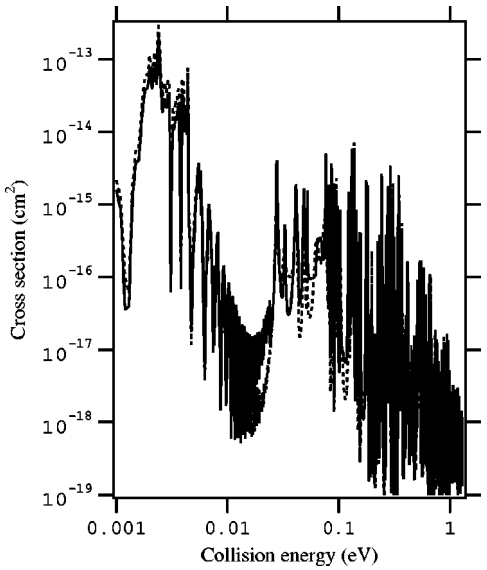

FIG. 3. DR cross section of ^4HeH ($v^+ = 0, N^+ = 0$). The adopted discretization interval of the dissociative states is 0.0007 a.u. for the solid curve and 0.0014 a.u. for the dotted curve.

In Sec. III A, we pointed out the arbitrariness of the AQD extrapolation to a large R, of which an example is shown by the solid and dashed curves in Fig. 1. The difference between the DR cross sections calculated by those two different AQD's is small, as shown by the solid and dashed curves in the $N^+ = 0$ graph in Fig. 4. This difference is only as much as 1%. We adopt the AQD of the solid curve to the present calculations hereafter.

Figure 4 shows the initial rotational-state dependence of the calculated DR cross section for the target ion of $^4HeH^+$ of $v^+ = 0$ and $N^+ = 0-3$. For a comparison, the result of calculation without a rotational transition is given by the dotted curve. This calculation was conducted by setting $M^{\sim}_{\ell\ell^+}(R) = \delta^{\sim}_{\ell\ell^+}$ and $\langle\Lambda|N^+\rangle^{J\ell^+\Lambda^+} = \delta_{N^+,J}$ in Eq. (14). It is clear that the rotational coupling makes a large resonance structure in the DR cross section and enhances the DR at a collision energy lower than 0.2 eV. Such a large enhancement does not appear for the hydrogen molecular ion, in which the DR is induced mainly by a potential curve crossing. The rotational-state dependence is quite strong on the rotationally induced resonance structure. The energy of the highest peak clearly changes with the initial rotational states at low energy. Those resonance states, which interact with the continuum states by the nonadiabatic interaction, depend on the initial vibration and rotation more sensitively than the electronic resonance states, as is seen in the DR of H_2^+ [13].

The cross section of $N^+ = 0$ shown in Fig. 3 is much different from the result obtained by Guberman [5]. Most of the calculated resonance structures could be identified into a vibrational v, rotational N, and principle quantum number n of the Rydberg state, where the incident electron is captured. The density of the resonance states is, however, quite large because of the infinite number of Rydberg states. Those Rydberg states are modulated by the vibronic and rotational nonadiabaticity.

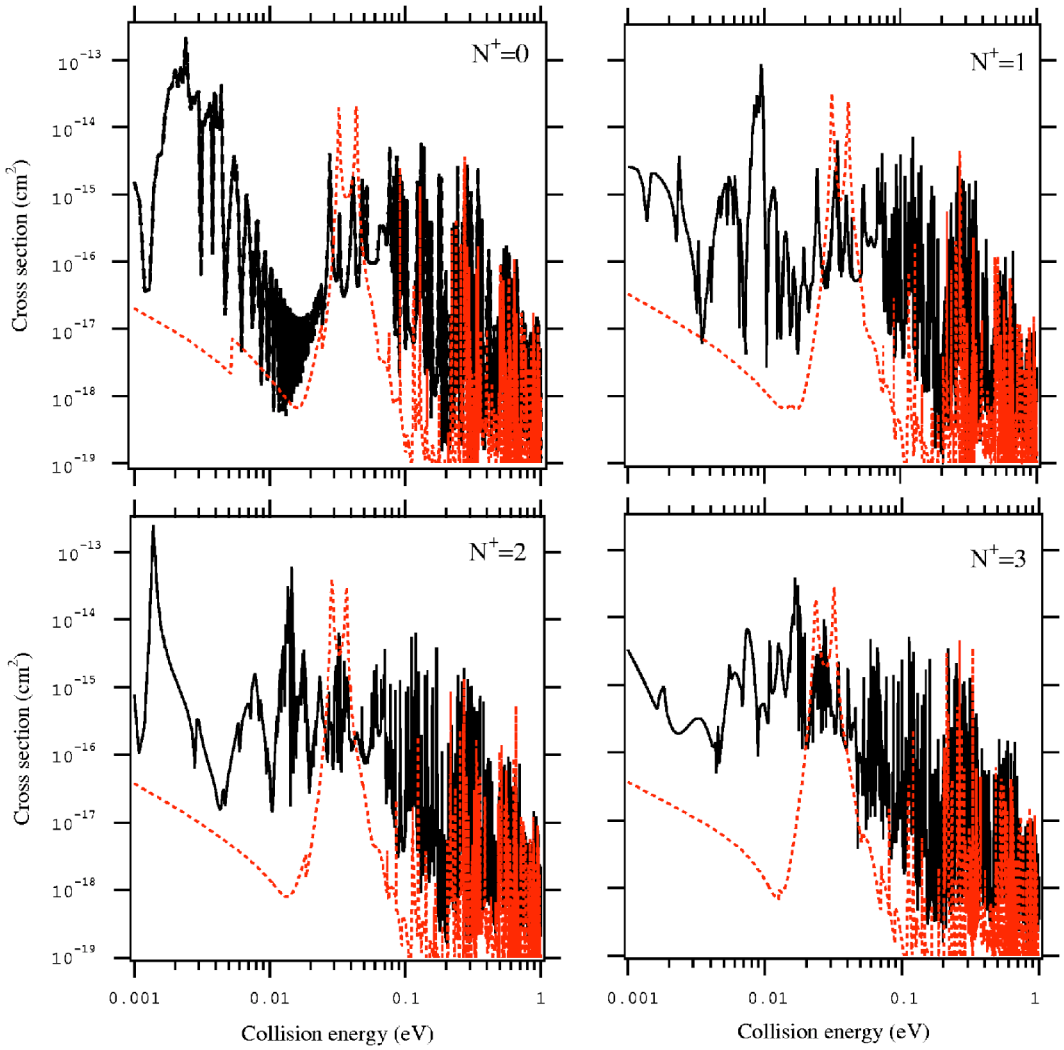

FIG. 4. DR cross section of $^4HeH^+$ for $v=0$. The rotational-state dependency is shown for $N^+=0-3$ by solid curves. The dotted curve indicates the cross section that ignored the rotational transition. In the graph of $N^+=0$, the calculation with the AQD of dushed curve in Fig. 1 is shown by the dashed curve, which coincides with the solid curve in the figure.

B. Comparison with experiment

The absolute values of the DR rate coefficients were measured by the CRYRING for $^3HeH^+$ and $^4HeH^+$ [3]. Figure 5 compares the calculated results with the experimental results. The calculated rate coefficient was convoluted by using Eq. (27) together with Eqs. (29) and (30). We here assumed the thermal distribution for the initial rotational states and fluctuation of incident electrons. The fluctuation temperatures are $T_\perp=10$ meV and $T_\parallel=0.5$ meV. For the initial rotational distributions of 300 K and 800 K, the DR rate coefficients were investigated.

The present calculation successfully reproduces the absolute values of the experimental rate coefficient, as shown in Fig. 5. The agreement is better for the higher initial rotational distribution temperature (800 K). Although more higher rotational temperatures should be investigated, this is the limit of the present study because the included rotational state is $N\leqslant 10$. Some specific features seen in the experiment are reproduced as the behaviors at low energies of two isotopes and some peak structures. On the other hand, some discrepancies are seen as the heights and positions of peaks. As a whole, the present calculation represents the character of difference between the two isotopes.

On $^4HeH^+$, two theoretical results were published and were compared with the experiment by the CRYRING [3]. One theoretical study is the *R*-matrix calculation by Sarpal, Tennyson, and Morgan [6]. The electronic parameters like the quantum defect employed in the present calculation are, in principle, based on the electronic states of their calculations. Another theoretical study is the MQDT calculation by Guberman [5], which was introduced in Sec. I. Although the present calculation has mentioned common points with these previous studies, the present DR cross sections are considerably different from those in these previous studies, and the consistency with experimental results is improved in the present calculation. The most specific point of the present is considering rotational motion, whereas it was neglected in the other studies. The present treatment of dynamics is sophisticated, as is the CDC included. As the result, the large absolute value of the experimental cross section is reproduced without the *X* state (the ground state of HeH), which

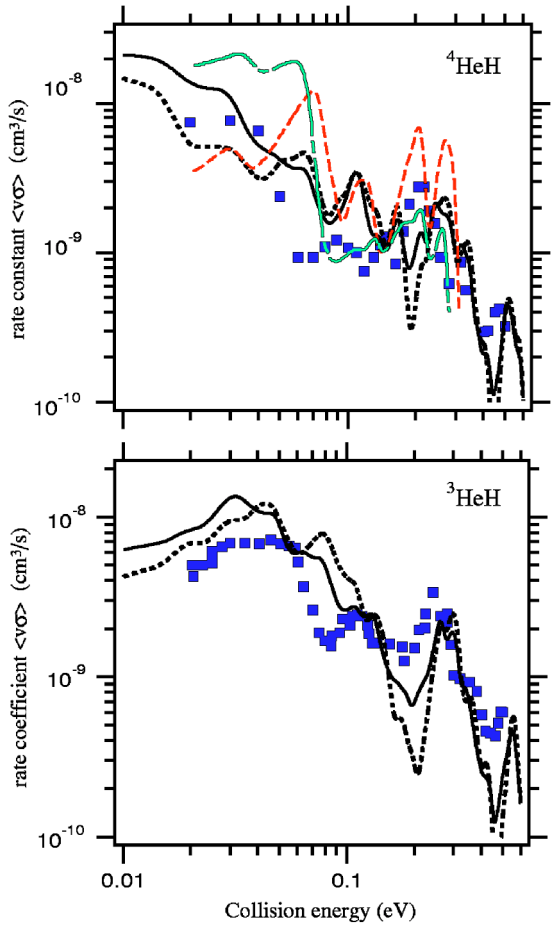

FIG. 5. Comparison of the DR rate coefficients of $^4HeH^+$ and $^3HeH^+$ with the experimental results by CRYRING [3]. The solid squares represent the experimental values. The present calculated values are convoluted by the thermal fluctuation of $T_\perp = 10$ meV and $T_\parallel = 0.5$ meV. Those initial rotational states were assumed to be distributed with the thermal distribution of 300 K (dotted curve) or 800 K (solid curve). The *R*-matrix calculation by Sarpal *et al.* [6] is shown by a dot-dashed curve, and the MQDT calculation by Guberman [4] is shown by a dashed curve. These two calculations are taken from the paper by Strömholm *et al.* [3].

made a major contribution to the DR in the *R*-matrix calculation [6].

Recently, the resolution of the experiment has been drastically improved by using the ultracold storage ring. We have already compared the present calculation with an experiment by TARN II for four isotopes of HeH^+ [7]. The comparison with TARN II measurements provides more detailed checking on the present calculation, although its rate coefficient is not absolute value but relative. Almost all structures of the experiment also appear in our calculation; however, an obvious discrepancy is seen in the relative magnitudes of some structures. The structures considerably depend on the distribution of the initial rotational states. The present calculation seems to support the higher rotational temperature 800 K as the analysis of CRYRING's result. The agreement between the present calculation and the experiments supports the validity of the present theoretical method. Based on this method, we shall discuss the mechanism of the DR in the following subsections.

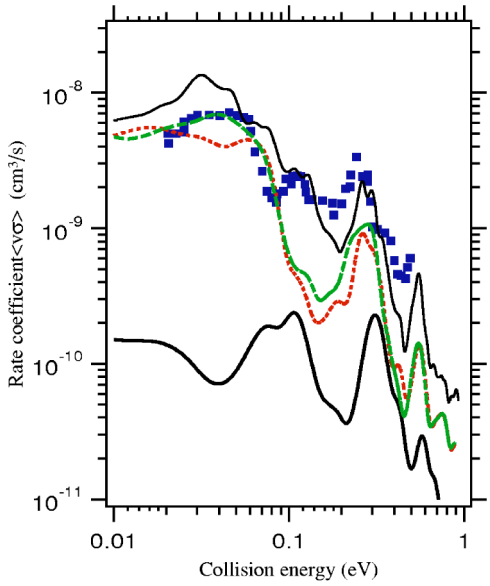

FIG. 6. Effect of AQD's jump and partial-wave mixing on the DR rate coefficient of $^3HeH^+$. The condition of electron fluctuation and the initial distribution of the rotational state are the same as in Fig. 5. The bold solid curve shows the no-jump calculation (see the text). The dotted curve indicates the calculation neglecting partial-wave mixing ($\chi = 0$), and the dashed curve represents the one assuming a complete mixing ($\chi = 1$). The thin solid curve and solid square are same as given in Fig. 5.

C. Enhancing mechanism

As was discussed in Sec. III B, the quantum defect of the $p\sigma$ state changes one unit with an internuclear distance. We call this change a jump of AQD. The internuclear dependence of the quantum defect causes the nonadiabatic interaction in the framework of the MQDT. Thus, a large enhancement of the DR is expected to be brought by the AQD jump.

In order to see the jump effect, we calculated the DR rate coefficient replacing the values of $p\sigma$ AQD by that of $p\pi$ AQD (see Fig. 1). We call this calculation a no-jump calculation. In Fig. 6, we compare the no-jump calculation with the present proper calculation. The rate coefficient magnitude of the no-jump calculation is one or two orders smaller than the proper one.

The jump of AQD $\mu(R)$ is the main factor enhancing the DR cross section in the noncrossing molecular system. This enhancement makes the DR cross section almost as large as that of the crossing existing system. This jump can be understood by investigating the correlation diagram. The antibonding molecular orbital ($p\sigma$) is constituted by the *ns* states of hydrogen and the ground state of helium atoms at the separated atom limit. The $p\sigma$ orbital correlates to the $(n+1)s$ state of the united atom limit (lithium) because the *ns* state is already occupied by a lower $p\sigma$ orbital. Thus, the AQD jumps. This principal quantum number change is not unusual for other molecules. For example, it is also seen in the I state

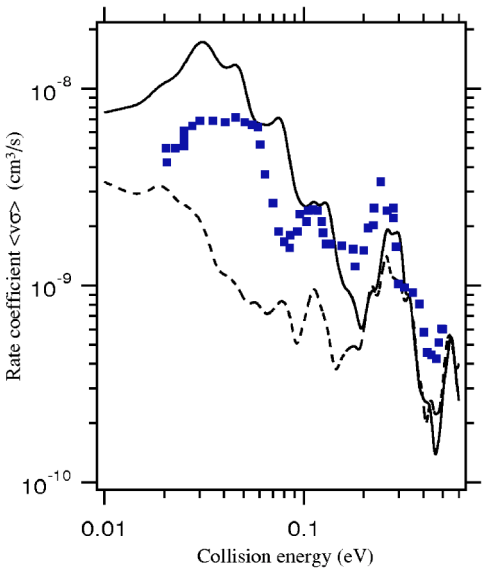

FIG. 7. Contribution of the CDC in the DR of $^3HeH^+$. The dashed curve indicates the result without the CDC. The solid curve and solid squares are the same as in Fig. 5.

$(3d\pi^1\Pi_g)$ of the hydrogen molecule. The point is whether or not the jump occurs within the Frank-Condon region of the initial vibrational state. In HeH*, the jump occurs near $R=1.3$ a.u., which is very close to the equilibrium point of HeH^+.

We want to point out that the enhancement by the jump still remains large for higher dissociation energy and for higher vibrational states. The integrand of the smoothed reactance matrix $\tilde{\mathcal{R}}$ given by Eq. (14) diverges at a certain R because of the jump of the quantum defect $\mu(R)$. The function $G(R)$ in Eq. (20) rapidly oscillates for the high-energy dissociative channels or highly excited vibrational states. The integration $I(=\tilde{\mathcal{R}})$ of Eq. (20) is usually small because of that oscillation if the integrand is not singular. The integration I always remains a finite value of the second term of Eq. (23) even for the limiting case of extreme oscillation.

Finally, we discuss the difference and similarity of the AQD jump compared with the electronic resonance in the crossing existing system. Both events induce a change of the principal quantum number of the adiabatic Rydberg states, when the internuclear distance changes across a certain distance. At that distance, the nuclear motion is distorted by the change of electronic character and exchanges the energies with electronic motion. In the electronic resonance scattering, the phase shift changes π radians when crossing over the resonance energy. In the noncrossing system, the phase shift of continuum electron does not change over π radians even if its energy changes at fixed nuclear distance. The AQD jump is clearly different from a resonance and induces the electron recombination only coupled with nuclear motion, whereas the electronic resonance itself induces the recombination.

D. Mixing of partial waves

We now investigate the effect of the mixing between the s and $p\sigma$ partial waves of the incident electron. Figure 6 shows the results of calculations setting the mixing parameter at $\chi=1$ and 0 in Eq. (25). Both calculations give the DR rate coefficient smaller than the proper calculation. This indicates that the R dependence of the mixing parameter enhances the DR. The recombined state of $p\sigma$ Rydberg states stabilizes owing to the transition to the s Rydberg states because the backward ionization is depressed by the transition to the s states, which are weakly coupled to the ionizing states. The strong mixing occurs near the classical turning point of dissociation ($R\sim0.9$ a.u.), where the avoided crossing between the s and $p\sigma$ AQD is seen in Fig. 1. The AQD jump point is near the equilibrium point of the molecular ion ($R\sim1.3$ a.u.). If the mixing occurred near the AQD jump, the DR rate might be small.

E. Closed dissociative channel

Figure 7 demonstrates the contribution of the CDC to the DR rate coefficient of $^3HeH^+$. At the energies lower than 0.2 eV, the CDC enhances the rate coefficient about half or one magnitude order. The structure is also largely affected by the CDC. The CDC improves the agreement with the experiment. When the employed CDC's are restricted to $\nu\leqslant2.25$, the calculated rate coefficient is affected very little by the restriction at the collision energies lower than 0.5 eV. This means that only the CDC near the energy of $n=2$ is important for the dissociation to H ($n=2$). The dissociative Rydberg states are well defined, although there is a distortion of the Rydberg states represented by the CDC.

V. CONCLUSION

We gave a detailed description of the MQDT, including the dissociative Rydberg and ionizing states. This method fairly succeeded in reproducing the experiment. It gives an answer to the mechanism of a large DR cross section in the crossing-absent system. The major mechanism is strong nonadiabatic coupling induced by the jump of the adiabatic quantum defect associating with the change of internuclear distance. It turned out that the rotational motion enhance the DR at a collision energy lower than 0.2 eV.

ACKNOWLEDGMENTS

The author would like to thank Dr. B. K. Sarpal for providing the details of his R-matrix calculations. He also thanks Professor T. Tanabe for imparting various information on the DR of HeH^+.

[1] D. R. Bates, Phys. Rev. **77**, 718 (1950); **78**, 492 (1950).
[2] A. E. Orel, K. C. Kulander, and T. N. Resigno, Phys. Rev. Lett. **74**, 4807 (1995).
[3] C. Strömholm *et al.*, Phys. Rev. A **54**, 3086 (1996).
[4] S. L. Guberman, Phys. Rev. A **49**, R4277 (1994); in *Atomic Collisions: A Symposium in Honor of Christopher Bottcher (1945–1983)*, edited by D. R. Schultz, M. R. Strayer, and J. H. Macek, AIP Conf. Proc. No. 347 (AIP, Woodbury, NY, 1995), p. 88.
[5] S. L. Guberman, in *The Physics of Electronic and Atomic Collisions*, edited by Louis J. Dubé, Brian A. Mitchell, J. William McConkey, and Chris E. Brion, AIP Conf. Proc. No. 360 (AIP, Woodbury, NY, 1995), p. 307.
[6] B. K. Sarpal, J. Tennyson, and L. A. Morgan, J. Phys. B **27**, 5943 (1994).
[7] T. Tanabe *et al.*, J. Phys. B **31**, L297 (1998); **32**, 5221(E) (1999).
[8] A. Giusti, J. Phys. B **12**, 3867 (1980).
[9] J. Semaniak *et al.*, Phys. Rev. A **54**, R4617 (1996).
[10] T. Tanabe *et al.*, Phys. Rev. A **49**, R1531 (1994).
[11] Ch. Jungen and O Atabek, J. Chem. Phys. **66**, 5584 (1977).
[12] H. Takagi, N. Kosugi, and M. Le Dourneuf, J. Phys. B **24**, 711 (1991).
[13] H. Takagi, J. Phys. B **26**, 4815 (1993).
[14] M. E. Rose, *Elementary Theory of Angular Momentum* (Wiley, New York, 1957), Sec. 3.
[15] M. J. Seaton, Rep. Prog. Phys. **46**, 167 (1983).
[16] H. Takagi, Phys. Scr. **T96**, 52 (2002).
[17] M. C. van Hemert and S. D. Peyerimhoff, J. Chem. Phys. **94**, 4369 (1991).
[18] B. K. Sarpal (private communication).
[19] N. F. Mott and H. S. W. Massey, *The Theory of Atomic Collisions* (Oxford University Press, New York, 1965), Sec. X.4.1.
[20] W. Kołos and J. M. Peek, Chem. Phys. **12**, 381 (1976).
[21] D. M. Bishop and L. M. Cheung, J. Mol. Spectrosc. **75**, 462 (1979).
[22] T. M. W. Crofton *et al.*, J. Chem. Phys. **91**, 5882 (1989).
[23] E. R. Cohen and B. N. Taylar, CODATA Bull. **60** (1986); reprinted in Rev. Mod. Phys. **59**, 1121 (1988).
[24] H. Danared, Phys. Scr. **T59**, 121 (1995).